A split ALFA tag-nanobody system for protein localization and proximity proteomics in mycobacteria

Allison Fay[1], Andrew P. Kurland[2,3], Zhuoning Li[4], Mara Monetti[4], Jeffrey R. Johnson[2,3], Michael S. Glickman[1,#]

1-Immunology Program, Sloan Kettering Institute
2- Department of Microbiology, Icahn School of Medicine at Mount Sinai, New York, NY, USA
3- Global Health and Emerging Pathogens Institute, Icahn School of Medicine at Mount Sinai, New York, NY, USA
4- Proteomics Innovation Laboratory, Sloan Kettering Institute

Memorial Sloan Kettering Cancer Center, 1275 York Avenue, New York, New York 10065 USA

#Correspondence:
glickmam@mskcc.org
1275 York Ave
New York, NY 10065
646-888-2368

Abstract

Tuberculosis remains a globally significant infection and new insights into the biology of *Mycobacterium tuberculosis* are badly needed. Discovery of protein localization and protein complex composition are powerful approaches to determine protein function, but have not been widely applied in mycobacteria, in part due to technical barriers. Here we develop a multi-functional system that utilizes the ALFA tag and functional protein fusions to an anti-ALFA nanobody (NBALFA) to target proteins in fast and slow growing mycobacteria. Insertion of the ALFA epitope tag on the target protein, coupled with conditional expression of the NBALFA fused to a fluorescent protein faithfully recapitulates cytosolic and membrane protein localization by fluorescent microscopy in living cells. Targeted NBALFA can relocalize an ALFA tagged protein to inclusion bodies or the cytoplasmic membrane, demonstrating enforced protein localization. Finally, conditional expression of the NBALFA fused to TurboID for proximity proteomics allowed identification of known partner proteins of the RNA polymerase complex and the PKS13 mycolic acid biosynthesis protein. We conclude that the split ALFA tag-nanobody system is a flexible platform for discovery protein biology in mycobacteria.

42 **Introduction**

43 *Mycobacterium tuberculosis* remains a high burden global health problem, infecting over
44 10.8 million people and causing 1.25 million deaths in 2023. There were about 400,000
45 estimated MDR/RR-TB cases in 2023 limiting the available drugs (1). Although our
46 knowledge of the biology of *M. tuberculosis* is expanding, we still lack a complete
47 understanding of the key processes in the mycobacterial cell, including cell wall
48 biosynthesis, transcription, and DNA replication. Understanding the biology of these
49 basic cellular systems is critical for the development of new antimicrobial therapies by
50 elucidating new drug targets or understanding how current therapies affect cell function.

51 Decades of development of genetic tools for mycobacteria have powered
52 directed and genome wide discovery approaches, including systems for genetic
53 deletion, integration, and point mutagenesis (2-4), CRISPRi technology for high
54 throughput library screening and targeted gene knockdown (5, 6), CRISPR gene
55 targeting for genetic deletions (7, 8), and approaches such as ORBIT which utilize
56 phage machinery to make multiple deletions and chromosomal integrations (9).
57 Although these advances in mycobacterial genetics have dramatically accelerated
58 discovery science for both pathogenic and nonpathogenic mycobacteria, proteomic
59 approaches to understand mycobacterial proteins in their native cellular context have
60 lagged. Protein fusions to a variety of functional proteins, including epitope tags,
61 fluorescent proteins, and chemically modifiable functional domains allow for
62 interrogation of protein spatial positioning, environment, and binding partners.
63 Localization via fluorescent protein fusions have elucidated a vast array of spatial
64 patterning within mycobacterial cells including, but not limited to asymmetric polar

growth elucidated by GFP-Wag31 localization (10), proteostasis machinery utilizing the tagged chaperone DnaK-mCitrine and disaggregase ClpB-mCitrine (11), and replication and architecture of the chromosome with tagged nucleoid-associated proteins, SSB-GFP and HupB-GFP (12, 13). High-throughput fusion libraries have also been developed to systematically assess protein patterning (14, 15). However, direct protein fusions to large partner proteins can introduce artifacts and impair protein function. For live cell localization, the most common fusion protein, GFP, though generally well tolerated, can impact folding, stability, and function due to its large size (16). GFP fusions can alter protein localization in live cells (17) and generally must be generated at the N- or C-terminus of the target.

Proximity proteomics is a powerful technique to investigate protein function by capturing both stable and transient protein interactions (18). The most commonly used systems fuse APEX/APEX2 (19, 20) or the BirA-derivatives, BioID/TurboID (21, 22), to a target protein of interest, thereby directing biotinylation to partner proteins in proximity. Recently, APEX-based proximity labeling was used in mycobacteria to identify the cytoplasmic and periplasmic compartment proteomes in Mtb (23, 24) and a BioID fusion was used to interrogate HbhA in *M. smegmatis* (25), but otherwise proximity proteomics has not been widely deployed in mycobacteria.

The ALFA tag is a rationally designed epitope tag that is small, balanced, alpha-helical, minimally reactive, and amenable to placement at the termini or internally in a target protein (26). Critically, a cognate nanobody (NBALFA), a single chain camelid antibody with picomolar binding affinity, was generated as a partner reagent for the ALFA tag (26). Because nanobodies efficiently fold and bind their target sequence within

88 the prokaryotic cell cytoplasm (27), the ALFA-NBALFA pair would potentially provide a
89 flexible system in which a single ALFA tagged target could be functionally targeted in
90 live mycobacterial cells by fusing partner proteins to the NBALFA. This manuscript
91 explores this idea and presents a multifunctional NBALFA/ALFA tag system for protein
92 studies in fast and slow growing mycobacteria.
93
94
95

Results

Nanobody based protein localization in *M. smegmatis*.

The design of the split ALFA system is presented in Figure 1. To test the utility of this approach, we generated chromosomal C-terminal ALFA tagged proteins by integrating the ALFA tag at the 3' end of the endogenous *rpoC* or *mmpL3* genes in *M. smegmatis*. These proteins are well characterized in mycobacteria with clear patterns of localization: RpoC to the nucleoid and MmpL3 to cell poles, (28-30). *M. smegmatis* MmpL3-ALFA and RpoC-ALFA were viable and had similar replication times in culture, indicating the ALFA tagged versions of both proteins were functional given that both genes are essential for viability. We verified expression of each ALFA tagged protein at the predicted size via immunoblot using NBALFA (Figure 2A). We then introduced plasmids encoding GFP translationally fused at the C-terminus to NBALFA with flexible linker (GGGSGGG) expressed from *ftsZ* (P_{ftsZ}) , *hsp60* (P_{hsp60}), or the Tet-inducible promoters into wildtype *M. smegmatis*, RpoC-ALFA, or MmpL3-ALFA. The protein levels of GFP-NBALFA correlated with expected promoter strength with P_{ftsZ} showing very little full length fusion protein compared to the P_{hsp60} driven construct (Figure 2B). Tet-inducible GFP-NBALFA was undetectable without inducer, but accumulated at its predicted size with anhydrotetracycline (ATc) induction (Figure 2B).

To determine if NBALFA can localize to ALFA tagged proteins in living cells, we imaged GFP-NBALFA by fluorescent microscopy in the absence or presence of an ALFA tagged target protein. Without an ALFA tagged protein, fluorescent signal from GFP-NBALFA was diffusely distributed and indistinguishable from free GFP (Figure 3A), with fluorescence signal intensity correlating to protein levels seen by immunoblot. We next assessed whether GFP-NBALFA would localize to ALFA tagged proteins *in vivo*. Mycobacterial RpoC-GFP was previously reported to co-localize to the nucleoid in logarithmically growing cells (28) and an RpoC-mCitrine fusion protein similarly colocalized with the irregular puncta of the nucleoid visualized by Hoechst staining (Figure 3B top panels). In RpoC-ALFA expressing cells, the nucleoid

123 localization pattern was weakly visible in cells co-expressing the GFP-NBALFA under P_{ftsZ} and
124 was easily visible when GFP-NBALFA was constitutively or inducibly expressed at higher levels
125 (Figure 3B). The pattern of GFP-NBALFA localizing to RpoC-ALFA was indistinguishable from
126 the direct RpoC-mCitrine fusion and contrasted with the diffuse pattern seen in cells not
127 expressing an ALFA-tagged protein. We repeated these experiments with MmpL3-GFP and
128 MmpL3-ALFA fusions. An MmpL3-GFP translational fusion accumulated at the poles and septa
129 as previously described (29, 30). Similarly, *M. smegmatis* cells expressing MmpL3-ALFA and
130 high levels of GFP-NBALFA (P_{hsp60} or Tet-induced) also showed a polar localization pattern that
131 was similar to the direct MmpL3-GFP fusion (Figure 3C). These results indicate that GFP-
132 NBALFA will localize to cytoplasmic or membrane proteins when co-expressed with an ALFA
133 tagged target.

134 **Protein Relocalization using NBALFA**

135 We next tested whether we could re-target an ALFA tagged protein to distinct subcellular
136 locations using NBALFA targeted to the membrane or a protein inclusion body. For inclusion
137 body targeting, we added the ELK16 aggregation sequence, which forms aggregates and
138 inclusion bodies *in vivo* (31), at the N-terminus of GFP-NBALFA to create ALFA tagged
139 fluorescent insoluble aggregates. When viewed by fluorescent microcopy, unlike the diffuse
140 cytoplasmic signal of GFP-NBALFA (Figure 3A), ELK16-GFP-NBALFA formed multiple foci in
141 the cell that occasionally coalesced into a large, polar inclusion bodies (Figure 4A). To test
142 whether ALFA tagged proteins would re-localize to these inclusion bodies, we coexpressed the
143 Tet-inducible ELK16-GFP-NBALFA with mCherry-ALFA or mCherry-HA. Upon induction of
144 ELK16-GFP-NBALFA and aggregate formation, mCherry-ALFA colocalized with GFP-NBALFA
145 puncta (Figure 4A, top). This relocalization was specific to the ALFA tag, as mCherry-HA
146 remained in a diffuse pattern when coexpressed with ELK16-GFP-NBALFA aggregates (Figure
147 4A, bottom).

148 To test whether NBALFA could relocalize an ALFA tagged protein to the membrane, we
149 utilized the first two transmembrane domains of *E. coli* MalF, which we previously used to mark
150 *M. smegmatis* membranes (11, 29). $MalF_{(1,2)}$-GFP-NBALFA localized in a membrane and septal
151 pattern in *M. smegmatis* (Figure 4B) and coexpression of mCherry-ALFA relocalized cherry
152 signal to the membrane (Figure 4B, top), whereas mCherry-HA remained in a diffuse
153 cytoplasmic pattern (Figure 4B, bottom). These experiments demonstrate that the split ALFA-NB
154 system can be used to relocalize proteins in living mycobacterial cells.

155 **Split ALFA nanobody based proximity proteomics in mycobacteria**

156 After confirming the NB based localization to ALFA tagged proteins in living *M. smegmatis*, we
157 adapted biotin-based proximity labeling to the split ALFA system. We chose the promiscuous
158 biotin-ligating enzyme, TurboID, which can label available lysines with biotin (21). We generated
159 a conditional expression vector encoding TurboID translationally fused to NBALFA (Figure 1).
160 When expressed in *M. smegmatis* RpoC-ALFA or MmpL3-ALFA, we were unable to detect
161 TurboID-NBALFA in uninduced cell lysates (Figure 5A). After induction for 3 hours with ATc, the
162 TurboID-NBALFA fusion protein was visible at the expected size when probed with an antibody
163 to BirA, (Figure 5A).

164 To determine if the TurboID-NBALFA fusion protein could catalyze biotinylation of an
165 ALFA tagged target, we developed a labeling protocol that would limit non-specific labeling by
166 employing transient expression of the TurboID-NBALFA fusion to allow localization to the ALFA
167 tagged target before initiation of labeling with biotin addition. However, mycobacterial cells
168 synthesize biotin (32, 33) and produce many biotinylated proteins (8, 34-36), indicating that
169 TurboID catalyzed biotinylation might proceed without biotin addition. To optimize conditions for
170 labeling, we measured TurboID-NBALFA dependent biotinylation in different media conditions.
171 Wild type *M. smegmatis* without TurboID has several dominant biotinylated proteins detected by
172 streptavidin-HRP (Figure S1). *M. smegmatis* expressing tet inducible TurboID-NBALFA in biotin
173 free Sauton's media with addition of inducer were indistinguishable from WT cells, indicating

174 that the endogenous biotin pool is not available for TurboID-NBALFA catalyzed biotinylation, at
175 least at this level of detection. However, expression of TurboID-NBALFA in LB media resulted in
176 detectable additional biotinylated proteins, and addition of biotin to Sauton's media resulted in
177 the highest level of additional biotinylation (Figure S1). These results indicate that there is
178 background endogenous biotinylation by TurboID in mycobacteria, but that biotin free media and
179 exogenous biotin addition can temporally restrict this background. However, these results also
180 emphasize the importance of the appropriate negative ALFA tagged control proteins to detect
181 specific biotinylation signals above both endogenously biotinylated proteins and those
182 nonspecifically biotinylated by TurboID.

183 To test the system in cells expressing an ALFA tagged target protein, we used TurboID-
184 NBALFA expressing cells carrying either RpoC-ALFA and MmpL3-ALFA. We observed
185 biotinylated proteins corresponding to the predicted sizes of the bait proteins, suggesting that
186 the TurboID-NBALFA was targeted to the ALFA tagged bait protein and subsequently labeled the
187 bait protein with biotin (Figure 5B). In addition, there were additional new biotinylated proteins in
188 the lysates each of the ALFA expressing cells compared to no ALFA control cells (Figure 5B),
189 suggesting proximity labeling of additional non-bait proteins above background. To identify
190 these additional biotinylated proteins, we isolated biotinylated proteins from RpoC-ALFA and no
191 ALFA control cells with streptavidin-agarose and quantitated peptides by mass spectrometry.
192 We identified the bait protein, RpoC, as a top hit enriched in the RpoC-ALFA strain when
193 compared to the no ALFA tag control strain (Figure 5C and Table S2). Furthermore, we identified
194 the core RNAP subunits RpoA (RNAPα) and RpoB (RNAPβ) as well as the transcription
195 termination protein, Rho as RpoC proximity hits (Figure 5C and Table S2).

196 **Proximity labeling in *M. tuberculosis*.**

197 To test proximity labeling using TurboID-NBALFA in *M. tuberculosis*, we targeted PKS13, a large
198 (186 kDa) multimodular protein essential for mycobacterial viability (37-39). PKS13 is essential
199 for mycolic acid biosynthesis and condenses the alpha branch fatty acids with the meromycolate

200 chain in the final steps of mycolic acid synthesis (37). Due to its distinct structural domains,
201 PKS13 is an ideal candidate to test the potential for domain specific proximity labeling by
202 placing the ALFA tag at distinct sites in the protein. The ALFA tag's small size and balanced α-
203 helical structure was reported to be tolerated at termini and at internal sites (26). We placed the
204 ALFA tag at the N-terminus, C-terminus, and two internal sites (552AA or 1357AA) in PKS13.
205 The internal sites were chosen for their predicted disordered structure between known
206 functional domains (39). To test the ability of different PKS13 ALFA tagged alleles to
207 complement the essential function of PKS13, we generated *M. bovis* BCG Δ*BCG_3862c* in a
208 merodiploid strain with a second copy of *rv3800c* (encoding *M. tuberculosis* PKS13) at the *attB*
209 site containing a nourseothricin resistance marker. L5 integrase catalyzed allelic exchange with
210 each ALFA-tagged PKS13 encoding plasmid conferring streptomycin resistance confirmed that
211 all four PKS13-ALFA alleles were functional (Figure S2).
212 To test PKS13 proximity labeling in *M. tuberculosis*, a constitutively expressed second
213 copy of *rv3800c*, the gene encoding PKS13, was integrated into the *M. tuberculosis*
214 chromosome. All *pks13* encoding alleles with distinct ALFA tag positions expressed an ALFA
215 tagged protein at the predicted size of PKS13, with subtle differences in PKS13 levels with
216 different tag positions, as compared to the DnaK loading control (Figure 6A). Coexpression of –
217 TurboID-NBALFA and subsequent biotin labeling revealed a high molecular weight streptavidin
218 reactive protein in all triplicate samples consistent with the expected size of PKS13, which was
219 not visible in the no ALFA control (Figure 6B). To identify biotinylated proteins dependent on the
220 ALFA-TurboID-NBALFA interaction, we purified biotinylated proteins from each of the labeled
221 lysates on streptavidin resin and quantitated peptides by mass spectrometry. PKS13 was the
222 top enriched protein identified by mass spectrometry in all four ALFA tag positions, indicating
223 proper targeting and labeling by TurboID-NBALFA, independent of tag position (Figure 6C,
224 Table S3). The PKS13 proximity interactome included multiple proteins with known functions in

225 mycolic acid biosynthesis including early Fas1 associated factors (AcpM, AccD6), FasII
226 components (InhA, HadB), mycolic acid methyltransferases that modify the meromycolate chain
227 (MmaA3, MmaA4), and proteins involved in TMM transport (CmrA) (Figure 6C, S3 and Table
228 S4). Additional proteins with relevance to the mycolic acid pathway were also detected (Figure
229 6C, Table S3), including proteins in the TAG lipid synthesis and lipid degradation pathways
230 (TGS1 and FadE23) whose products can be used for mycolic acid synthesis, (40-42). We also
231 identified protein chaperones, including DnaK, which we previously implicated as required for
232 large multimodular protein stability in *M. smegmatis* (11). To determine if distinct ALFA tag
233 positions within PKS13 led to distinct biotinylation patterns, we compared the proximity
234 interactome of PKS13 alleles with different ALFA tagged positions. This analysis revealed a core
235 PKS13 interactome shared in all four ALFA tagged PKS13 positions (Figure 6D, Table S5), but
236 also revealed proximity hits unique to each tag position, particularly for the 1352AA tag position,
237 indicating that ALFA tag placement can reveal distinct protein interactors in large multidomain
238 proteins.

Discussion

We have created a flexible split ALFA tag-ALFA nanobody based system for protein-based discovery science in mycobacteria. The core enabling technology of this system is the ALFA tag/NBALFA pair. The high affinity of the NBALFA for the ALFA tag, combined with the ability to express the single chain in living bacterial cells, enables our approach of using the NB as a delivery vehicle to localize distinct functional protein partners to an ALFA tagged protein of interest. This design gives tremendous flexibility as it allows a single bacterial strain bearing an ALFA tagged protein of interest to be used for protein localization, affinity purification, and proximity proteomics, simply by changing the fusion partner of the expressed NBALFA. The split design of the system may offer several advantages in addition to this flexibility. The small size and optimized structural design of the ALFA tag is presumably less likely to artifactually perturb protein function or localization than a larger direct fusion such as a fluorescent protein or TurboID. The functionalized NB can also be conditionally expressed, allowing temporal control of the imaging or proximity output to coincide with experimental conditions. We demonstrate the utility of the system for visualizing the subcellular distribution of both cytoplasmic and membrane proteins by fluorescent microscopy; for tethering a protein to a specific subcellar compartment; and for proximity proteomics. This latter usage, proximity proteomics, provides a new system to interrogate protein complexes in mycobacteria. Although APEX based proximity proteomics has been applied in mycobacteria for the periplasmic and cytoplasmic compartment, this system is less amendable to cytoplasmic labeling has not been demonstrated for a specific protein target (23, 24, 43). In contrast, the NBALFA system should be useful for cytoplasmic proteins and membrane proteins if targeted to the cytoplasmic domains of those membrane proteins. We also note that the ALFA tag can also be used directly for affinity purification of protein complexes, with or without crosslinking, providing an approach for structural characterization of native protein complexes purified directly from mycobacteria.

264 We can envision several future uses of this system for discovery biology in
265 mycobacteria. It would be possible with this system to interrogate the proximity interactome of
266 an entire pathway by ALFA tagging a set of proteins with sequential steps in the pathway.
267 Similarly, the dynamic protein interactome of *M. tuberculosis* antibiotic targets could be
268 interrogated during drug treatment or other exogenously applied cellular stress. Similarly,
269 additional functional domains could be fused to NBALFA to enable additional discovery
270 approaches, such as HaloTag for small molecule labeling. We also envision that this approach
271 may be generally applicable to other bacterial or eukaryotic systems in which the flexibility of the
272 split ALFA approach would offer similar advantages.
273

274 **Methods**

275 **Growth conditions.**

276 *M. smegmatis* strains were cultured in LB with 0.5% glycerol, 0.5% dextrose, and 0.05% Tween
277 80 (LB_{smeg}) or Difco Middlebrook 7H9 supplemented with 0.2% glycerol, 10% ADS (0.5%
278 albumin, 0.085% NaCl, 0.2% dextrose) and 0.05% Tween 80 (7H9). *M. bovis* BCG Pasteur
279 strains were cultured in Difco Middlebrook 7H9 supplemented with 0.2% glycerol, 10% ADS
280 (0.5% albumin, 0.085% NaCl, 0.2% dextrose) and 0.05% Tween 80 (7H9) or on Difco
281 Middlebrook 7H10 agar plates were supplemented with 0.2% glycerol and 10% (wt/vol)
282 Middlebrook oleic acid-albumin-dextrose-catalase (OADC). *M. tuberculosis* Erdman strains were
283 cultured in Difco Middlebrook 7H9 supplemented with 0.2% glycerol and 10% (wt/vol)
284 Middlebrook oleic acid-albumin-dextrose-catalase (OADC) and 0.05% Tween 80 (7H9) or on
285 Difco Middlebrook 7H10 agar plates were supplemented with 0.2% glycerol and 10% (wt/vol)
286 Middlebrook oleic acid-albumin-dextrose-catalase (OADC). Sauton's media was utilized for
287 biotin-free conditions.

288

289 **Bacterial and DNA manipulations**

290 Standard procedures were used to manipulate recombinant DNA and to transform *E. coli*. *M.*
291 *smegmatis* strains were derivatives of mc2155 (44). *M. bovis* BCG Pasteur and *M. tuberculosis*
292 Erdman were also used. Gene deletions were made by double stranded DNA recombineering
293 (3). All strains used in this study are listed in Table S1. Plasmids including relevant features,
294 and primers are listed in Table S1. *M. smegmatis*, *M. bovis BCG*, and *M. tuberculosis* were
295 transformed by electroporation (2500V, 2.5μF, 1000Ω). Antibiotic concentrations used for
296 selection of mycobacterial strains were as follows: kanamycin 20 μg/ml, hygromycin 50 μg/ml,
297 streptomycin 20 μg/ml, nourseothricin 25 μg/ml.

298

299 **Immunoblotting**

300 For protein and epitope tag detection, the following antibodies were used: GFP (Rockland
301 Immunochemicals, Rabbit Anti-GFP polyclonal antibody, 1 mg/ml, 1:20,000), SigA (purified anti-
302 SigA from rabbit sera, 1:10,000) (45), TurboID (Invitrogen, BirA Polyclonal Antibody, 1mg/ml,
303 1:10,000), DnaK (anti-DnaK rabbit poly clonal sera, 1:10,000) (46), ALFA tag (purified NBALFA
304 1mg/ml, 1:5000 and Genscript, Rabbit anti-VHH HRP conjugated antibody, 1:10,000).

305

306 **NBALFA Purification**

307 The sequence encoding the ALFA tag binding nanobody was cloned with a C-terminal 6histidine
308 tag into an IPTG inducible construct, PelB leader-containing derivative of pET21b and
309 expressed and purified as described (47) with the following modifications. A 19-hour induction
310 was done at 22 degrees C in BL21(DE3) cultured in Terrific Broth containing carbenicillin
311 (100ug/ml). Eluates were pooled, concentrated in Amicon Ultra-4 3k, and run on Superdex 200
312 10/300 size exclusion column using an AKTA purifier in PBS. Nanobody was stored at
313 concentrations of 1-10mg/ml in PBS containing 20% glycerol at -80C.
314
315 **Microscopy**
316 All images were acquired using a Zeiss Axio Observer Z1 microscope equipped with Definite
317 focus, Colibri2.0 and Illuminator HXP 120 C light sources, a Hamamatsu ORCA-Flash4.0
318 CMOS camera, and a Plan-Apochromat 100×/1.4 numerical aperture oil differential inference
319 contrast (DIC) lens objective. Zeiss Zen software was used for acquisition and image export.
320 The following filter sets and light sources were used for imaging: GFP (38 HE, Colibri2.0 470
321 light-emitting diode [LED]), yellow fluorescent protein (YFP) (46 HE, Colibri2.0 505 LED) and
322 DAPI (49, HXP 120 C). For cell staining a final concentration of 200uM Hoechst (Hoechst
323 33342 Solution (20 mM), ThermoScientific) was added and cells were incubated for 10 minutes
324 at 37 degrees. Cells were pelleted by centrifugation at 3,000 × g for 1 min. Supernatant was
325 removed and cells were resuspended in 50 µl of PBS. For single-time-point live-cell imaging, 2
326 µl of culture was spotted onto a 1.5% low-melting-point agarose pad made in a final
327 concentration of PBS with 0.2% glucose. For pad preparation, agarose was heated to 65°C and
328 poured into a FastWell incubation chamber (Grace Bio-labs, 18x18mm, 1mm depth) pressed
329 onto a 25-mm by 75-mm glass slide. A second slide was pressed down on top, and the setup
330 was allowed to cool at room temperature for 10 min. The top slide was removed, and two
331 microliters of *M. smegmatis* culture was added to the pad then topped with a coverslip
332 (18x18mm, No 1.5).
333
334 **Proximity labeling, lysate preparation, and biotinylated protein capture**
335 From a log phase starter culture (OD600 0.3-0.6), 3x30ml cultures for each strain were
336 prepared in 60ml inkwell bottles (Nalgene, #342020-060) targeting a final OD600 of 0.3 after
337 18hrs (*M. smegmatis*) or 48hs (Mtb). For *M. smegmatis* RpoC-ALFA proximity labeling, the
338 following strains were used: MG7085 (No ALFA tag control) and MGM7106 grown in 30mls
339 LBsmeg with kanamycin 20ug/ml. For Mtb PKS13-ALFA experiment: MGM7416, MGM7418,
340 MGM7419, MGM7420, MGM7421 were grown in 30ml 7H9OADC with kanamycin 20µg/ml.

341 Cultures were washed with 10ml Sauton's media (biotin-free media) then resuspend 30ml
342 cultures in Sauton's media with kanamycin in fresh 60ml inkwell bottle and grown at 37C
343 shaking at 150rpm (6h *M. smegmatis*, 24h Mtb) followed by addition of ATc-50ng/ml (3h *M.*
344 *smegmatis*) or ATc-100ng/ml (18h Mtb). Cells were collected by centrifugation at 3700xG for
345 10min at room temperature and resuspended in 2ml Sauton's media (no ATc/no kanamycin) and
346 transferred to 2ml O-ring sealed tube, collected by centrifugation at 3700xG for 5min at room
347 temperature, and resuspended in 1ml Sauton's media. Cultures were incubated for 2hrs with
348 200μM Biotin (Sigma, B4501) with shaking at 37C and then collected by centrifugation at
349 20,000xG for 1min at 4C and placed immediately on ice. Cell pellets were washed with 2ml cold
350 TBS (20mM Tris, 150mM NaCl, pH 7.5), then collected by centrifugation at 20,000xG for 1min at
351 4C and cell pellets frozen at -20 degrees C.
352 For lysate preparation, frozen cell pellets were thawed on ice and resuspended with
353 250ul bead mix (1:1 mix, Biospec 11079101z and 1079107zx) and 1ml cold TBS with protease
354 inhibitors (PI) (Pierce, PIA32955). Lysis was performed by mechanical disruption 3X45 seconds
355 (Biospec Minibeadbeater) with 5 min icing between runs. Unbroken cells/debris were collected
356 by centrifugation at 20,000xG for 1min at 4C, supernatants collected, and residual pellets lysed
357 again with beads and 400ul cold TBS with protease inhibitors. Pooled supernatants were mixed
358 with 150ul of 10x RIPA buffer detergents (TBS+ 10% triton x-100, 1% SDS, 5% sodium
359 deoxycholate) and mixed by inversion, centrifuged at 20,000xG for and (for Mtb) the
360 supernatant was filtered twice through EMD Millipore™ Ultrafree™-CL Centrifugal Filter Devices
361 with Durapore™ Membrane to remove any residual *M. tuberculosis*. For biotinylated protein
362 capture, protein lysates were mixed with 80ul of Streptavidin-Agarose (GoldBio, S-105-10)
363 prewashed 3X in 1ml TBS and incubated rotating at 4C for 18h. Agarose beads were collected
364 at 250xG for 1min at 4C and washed 2xs with 1ml RIPA/SDS (TBS+ 0.1% triton x-100, 0.1%
365 SDS, 0.5% sodium deoxycholate) followed by 4 washes with TBS.
366
367 **Peptide preparation for Mass Spectrometry**
368 Streptavidin-agarose beads were resuspended in 40ul of 2M urea, 50mM tris pH 8.0 then 0.4ul
369 of 100mM DTT was added to each sample. Beads were incubated at 37C for 30 min with
370 shaking then 0.3ul 500mM iodoacetamide was added and beads were incubated at room
371 temperature for 45 min protected from light. 0.3ul 500mM DTT was added then 750ng of trypsin
372 protease (Pierce, 90057) and beads were incubated overnight shaking at 37C. Beads were
373 spun down 250xG 2min and supernatant was transferred to a new tube. 500ng of trypsin was
374 added to the supernatant and incubated for 2h at 37C with shaking. Samples were then

375 acidified with trifluoroacetic acid (TFA) to a final concentration of 0.1%. 200ul of 80% acetonitrile
376 (ACN), 0.1% TFA was added to a BioPureSPN Mini C18 spin columns (Nest Group, Product #
377 HUM S18R) and spun at 100 x G for 1 min. 200ul of 0.1% TFA was added to the column and
378 spun 100xG for 1 min, then repeated. The digested sample was then added to the column and
379 spun 100xG for 1 min. 200ul of 0.1% TFA was added to the column and spun 100 x G for 1 min,
380 then repeated. The column was then placed in a fresh tube and peptides were eluted with 100ul
381 40% ACN, 0.1% TFA and spun 100 x G for 1 min. Peptides were dried in a speedvac.
382
383 **Mass spectrometry data acquisition**
384 Samples were analyzed on an Orbitrap Eclipse mass spectrometry system equipped with an
385 Easy nLC 1200 ultra-high pressure liquid chromatography system interfaced via a Nanospray
386 Flex nanoelectrospray source (Thermo Fisher Scientific). Samples were injected onto a fritted
387 fused silica capillary (30 cm × 75 μm inner diameter with a 15 μm tip, CoAnn Technologies)
388 packed with ReprosilPur C18-AQ 1.9 μm particles (Dr. Maisch GmbH). Buffer A consisted of
389 0.1% Formic Acid (FA), and buffer B consisted of 0.1% FA/80% ACN. Peptides were separated
390 by an organic gradient from 5% to 35% mobile buffer B over 120 min followed by an increase to
391 100% B over 10 min at a flow rate of 300 nL/min. Analytical columns were equilibrated with 3 μL
392 of buffer A.
393 To build a spectral library, samples from each set of biological replicates were pooled
394 and acquired in data-dependent manner. Data-dependent acquisition (DDA) was performed by
395 acquiring a full scan over a *m/z* range of 375-1025 in the Orbitrap at 120,000 resolving power
396 (@ 200 *m/z*) with a normalized AGC target of 100%, an RF lens setting of 30%, and an
397 instrument-controlled ion injection time. Dynamic exclusion was set to 30 seconds, with a 10
398 p.p.m. exclusion width setting. Peptides with charge states 2-6 were selected for MS/MS
399 interrogation using higher energy collisional dissociation (HCD) with a normalized HCD collision
400 energy of 28%, with 3 seconds of MS/MS scans per cycle.
401 Data-independent analysis (DIA) was performed on all individual samples. A full scan
402 was collected at 60,000 resolving power over a scan range of 390-1010 *m/z*, an instrument
403 controlled AGC target, an RF lens setting of 30%, and an instrument controlled maximum
404 injection time, followed by DIA scans using 8 m/z isolation windows over 400-1000 *m/z* at a
405 normalized HCD collision energy of 28%.
406
407 **Mass spectrometry data analysis**

408 The Spectronaut algorithm was used to build spectral libraries from DDA data, identify
409 peptides/proteins, localize phosphorylation sites, and extract intensity information from DIA data
410 (48). DDA data were searched against the *Mycobacterium tuberculosis* or *M. smegmatis*
411 reference proteome sequences in the UniProt database (one protein sequence per gene,
412 downloaded on June 13, 2022). False discovery rates were estimated using a decoy database
413 strategy (49). All data were filtered to achieve a false discovery rate of 0.01 for peptide-
414 spectrum matches, peptide identifications, and protein identifications. Search parameters
415 included a fixed modification for carbamidomethyl cysteine and variable modifications for N-
416 terminal protein acetylation, methionine oxidation, and for phosphoproteomics samples, serine,
417 threonine, and tyrosine phosphorylation. All other search parameters were Biognosys factory
418 defaults.
419 Statistical analysis of proteomics data was conducted utilizing the MSstats package in R
420 (50). All data were normalized by equalizing median intensities, the summary method was
421 Tukey's median polish, and the maximum quantile for deciding censored missing values was
422 0.999.
423

424 **Acknowledgements**
425
426 This work was funded by P30 AI168433 (Tri-I TRAC) and P30 CA08748.
427

428 **Conflicts of Interest**
429 MSG declares equity and consulting fees from Vedanta biosciences and consulting fees from
430 Fimbrion therapeutics.
431

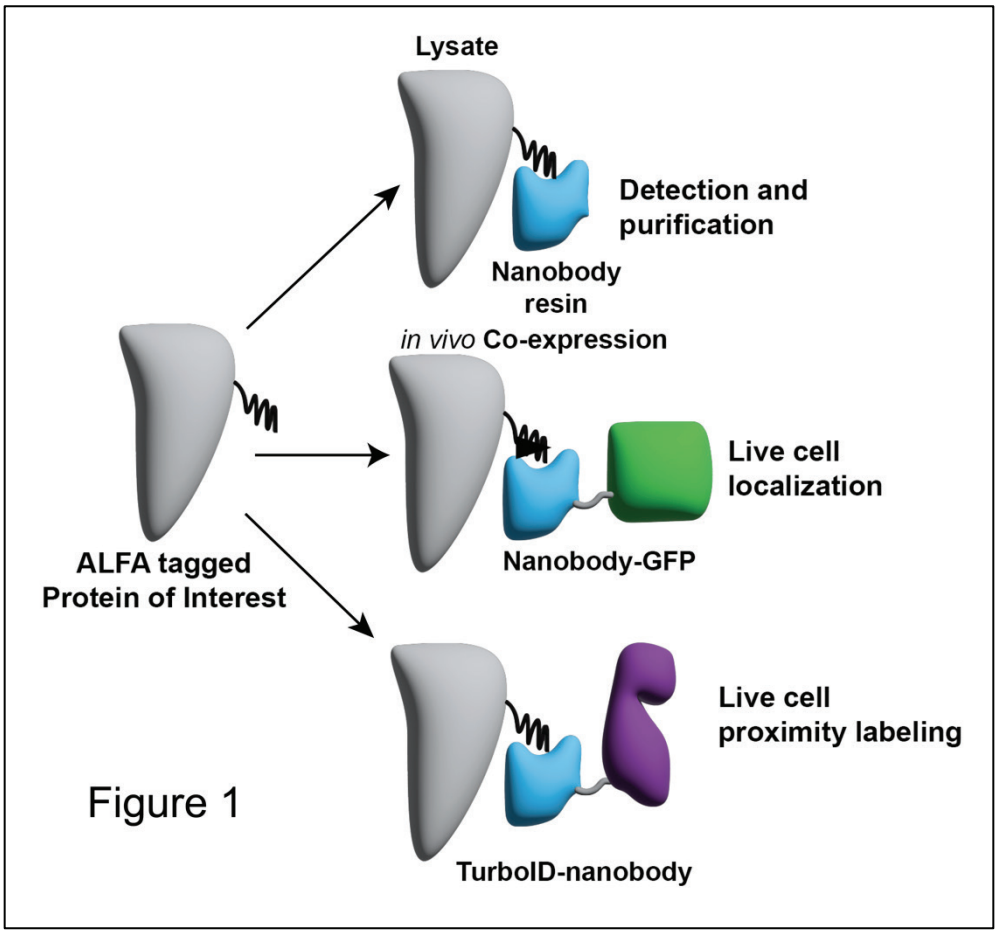

Figure 1. Design of a split ALFA tag nanobody system for detection/purification, localization, and proximity labeling in mycobacteria

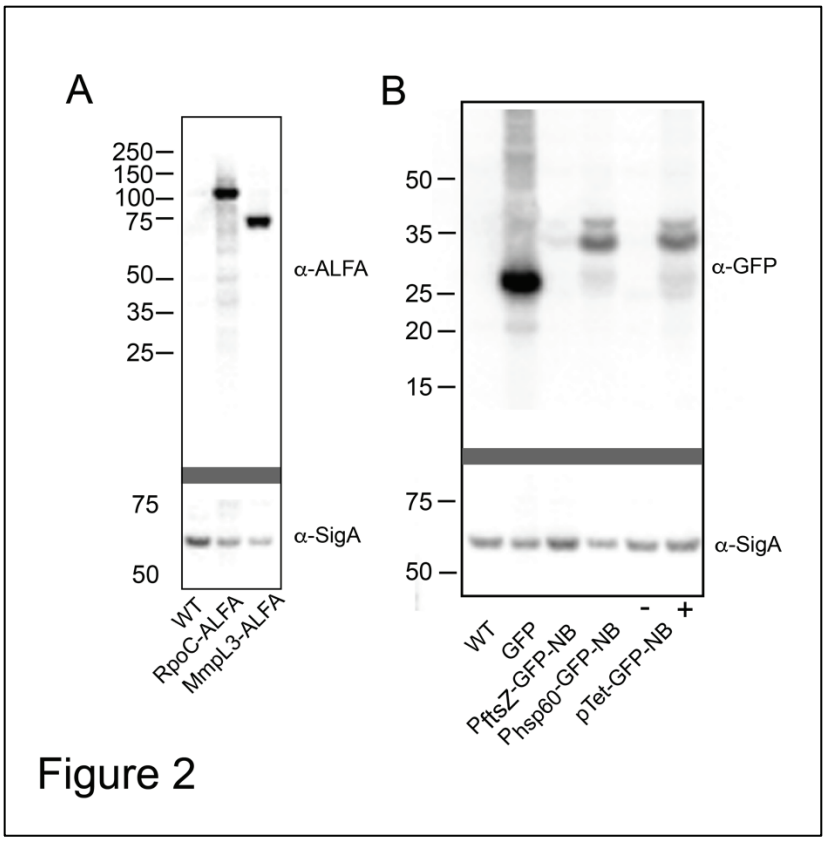

Figure 2. Chromosomal ALFA tagged MmpL3 and RpoC

(A) Immunoblots of lysates from MC2155 (WT), MGM7103 (encoding RpoC-ALFA), and MGM7059 (encoding MmpL3-ALFA). The top blot is probed using NBALFA and anti-VHH-HRP. The bottom blot stripped and probed with anti-SigA and anti-rabbit Ig-HRP as a loading control.

(B) Immunoblots of lysates from MC2155, MGM6970 (expressing GFP), MGM7087 (expressing GFP-NBALFA from the P_{ftsZ1} promoter), MGM7089 (expressing GFP-NBALFA from the P_{hsp60} promoter), MGM7047 (expressing TetON GFP-NBALFA, no ATc), and MGM7047 (encoding TetON GFP-NBALFA, + ATc-50ng/ml). Top blot probed with anti-GFP and anti-rabbit Ig-HRP. Bottom blot stripped and probed with anti-SigA and anti-rabbit Ig-HRP.

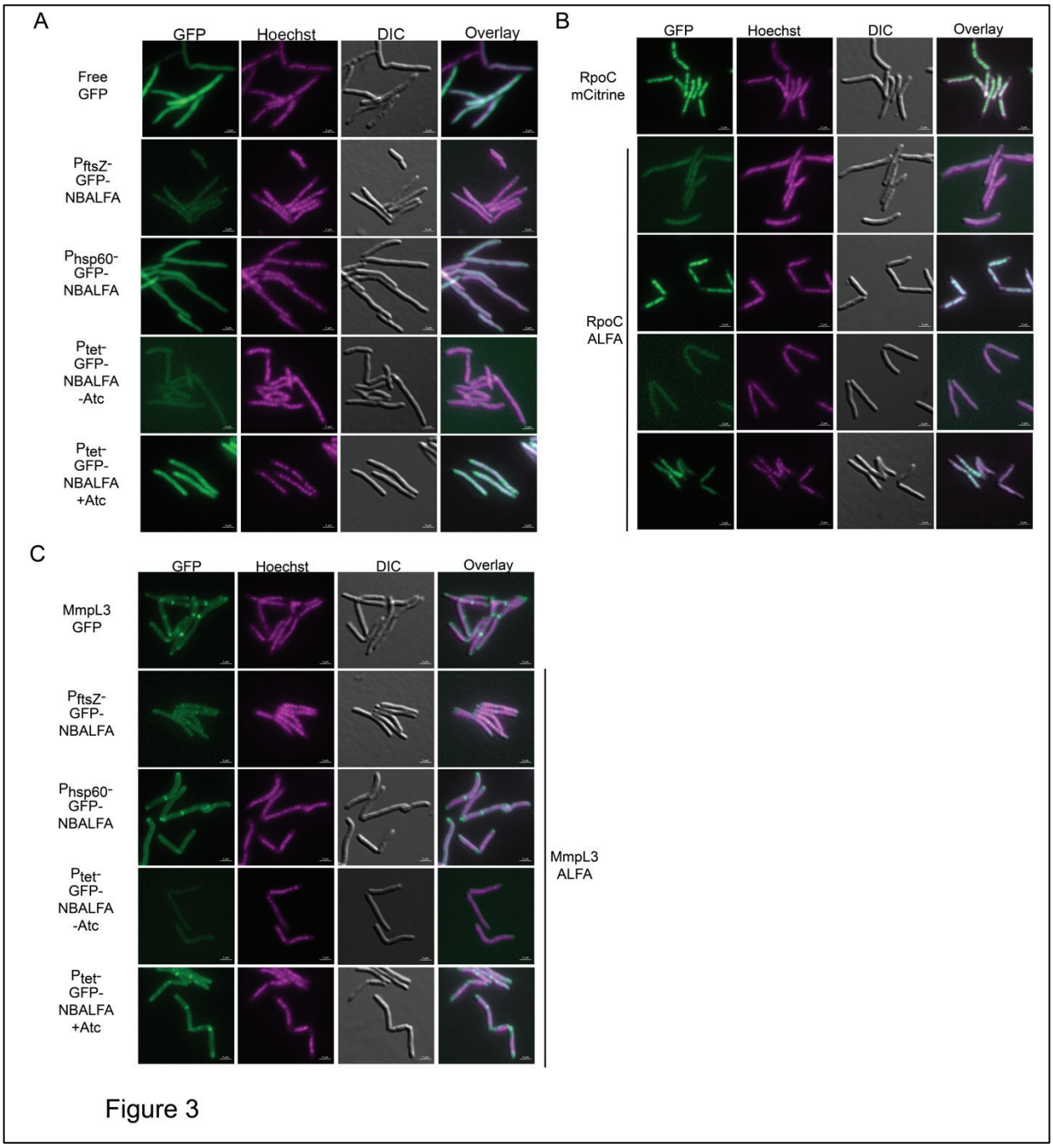

Figure 3. Detection of protein localization in live mycobacterial cells using split NBALFA (**A**) GFP-NBALFA mimics the distribution of free GFP in the absence of an ALFA tagged target protein. MGM6970 (expressing free GFP), MGM7087 (expressing GFP-NBALFA from P_{ftsZ1}), MGM7089 (expressing GFP-NBALFA from P_{hsp60}), MGM7047 (expressing TetON GFP-NBALFA, no ATc), MGM7047 (encoding TetON GFP-NBALFA, + ATc-50ng/ml).

457 **(B)** NBALFA localizes to RpoC in living cells. MGM6026 (expressing an RpoC-mCitrine protein
458 fusion), MGM7107 (expressing RpoC-ALFA and GFP-NBALFA under P_{ftsZ1}), MGM7108
459 expressing RpoC-ALFA and GFP-NBALFA under P_{hsp60}), MGM7105 (expressing RpoC-ALFA
460 and TetON GFP-NBALFA, no ATc), MGM7105 (expressing RpoC-ALFA and TetON GFP-
461 NBALFA, + ATc-50ng/ml).
462 **(C)** NBALFA localizes to MmpL3 in living cells. MGM6464 (expressing a MmpL3-GFP fusion),
463 MGM7099 (expressing MmpL3-ALFA and GFP-NBALFA under P_{ftsZ1}), MGM7101 (encoding
464 MmpL3-ALFA and GFP-NBALFA under P_{hsp60}), MGM7081 (expressing MmpL3-ALFA and TetON
465 GFP-NBALFA, no ATc), MGM7081 (expressing MmpL3-ALFA and TetON GFP-NBALFA, + ATc-
466 50ng/ml).
467
468 All images contain 2uM scale bar and show GFP (imaged 500ms, 70% Colibri LED), Hoechst
469 staining (DAPI, 500ms external lamp), DIC, and overlay.
470

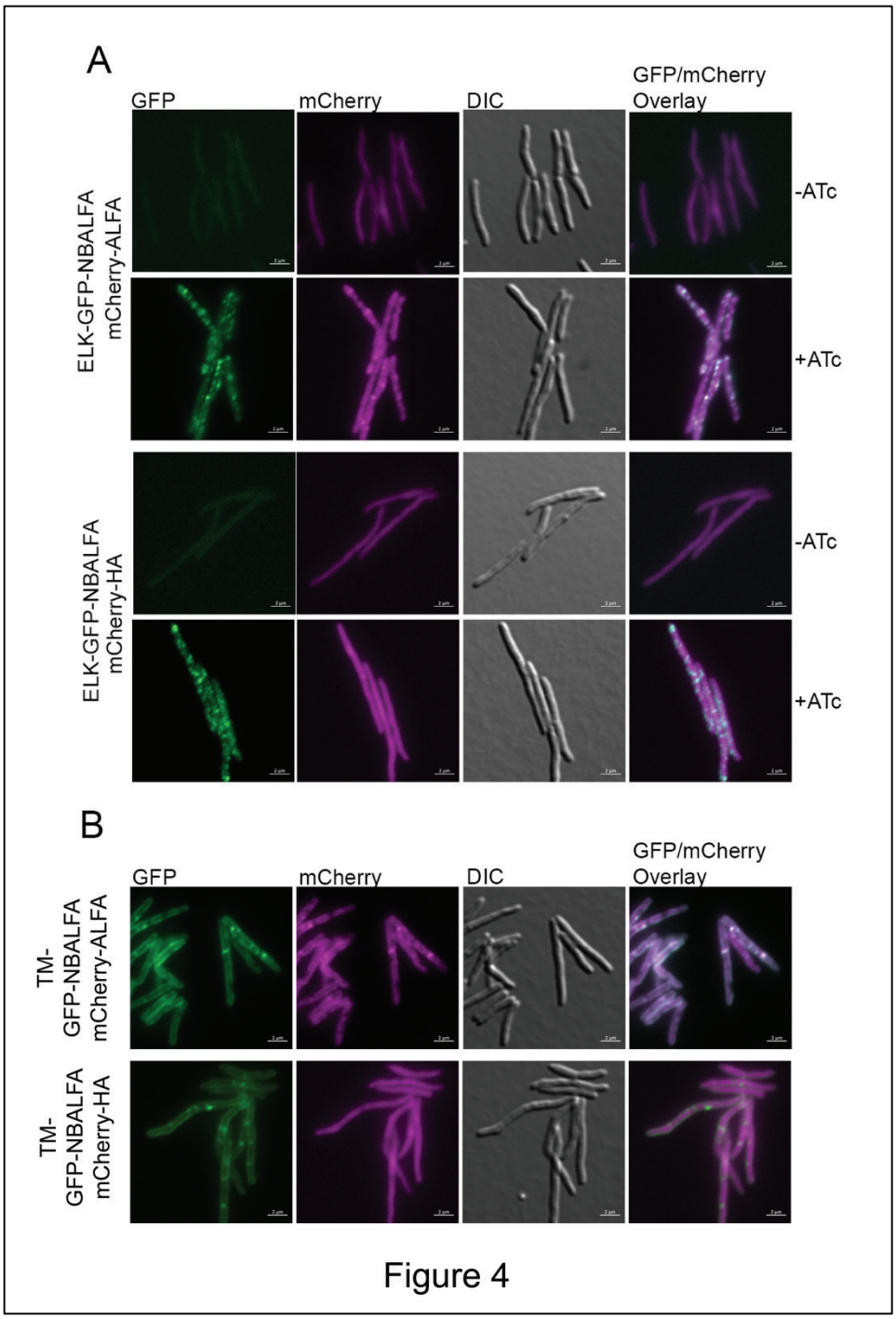

Figure 4. Enforced protein relocalization using split NBALFA

(A) Relocalization to inclusion bodies. Top section: AFM1996 (mCherry-ALFA, TetON ELK16-GFP-NBALFA) without (top) and with (bottom) ATc showing GFP inclusion body formation and colocalization of mCherry-ALFA to inclusions. Bottom section, same as (A), but with a control

477 mCherry-HA expression strain, AFM1995 (mCherry-HA, TetON ELK16-GFP-NBALFA) without
478 (top) and with (bottom) ATc to induce GFP inclusion bodies.
479 (B) Relocalization to the membrane. mCherry-ALFA, or control mCherry-HA, with coexpression
480 of an inducible membrane targeted $MalF_{(TM1,2)}$-GFP-NBALFA. Top section: MGM7879 (mCherry-
481 ALFA, TetON $MalF_{(TM1,2)}$-GFP-NBALFA) with ATc. Bottom section: MGM7985 (mCherry-HA,
482 TetON $MalF_{(TM1,2)}$-GFP-NBALFA) with ATc.
483
484 All images contain 2uM scale bar and show GFP (imaged 500ms, 70% Colibri LED), mCherry
485 (imaged 500ms, 70% Colibri LED), DIC, and GFP/mCherry overlay.
486
487

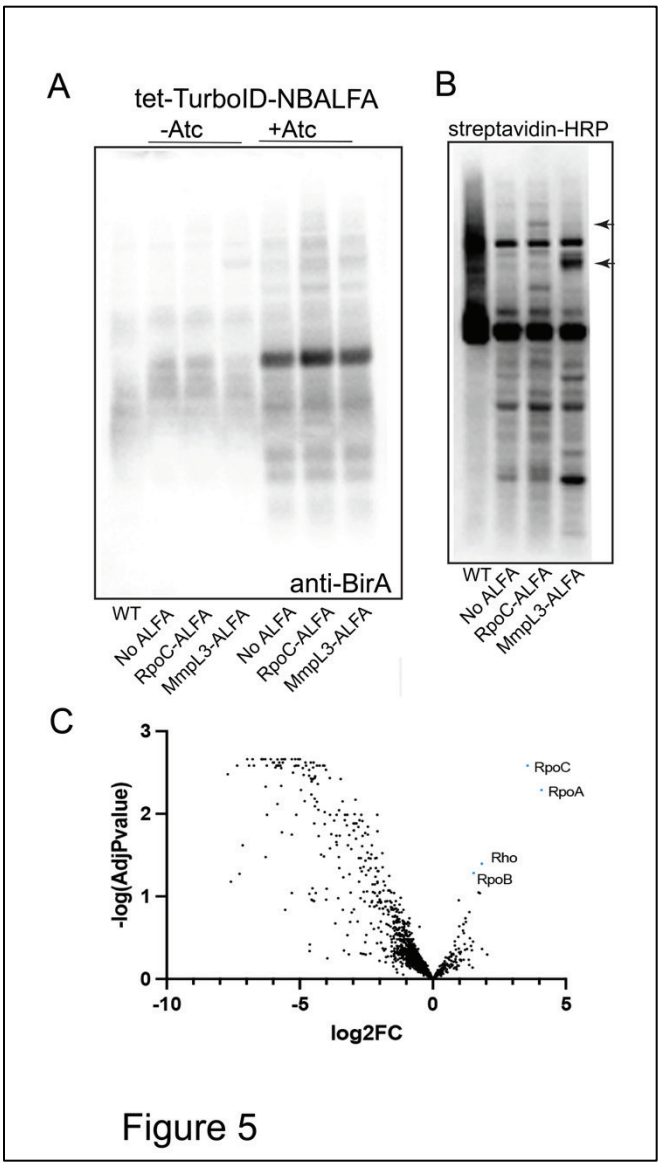

Figure 5. Proximity labeling in *M. smegmatis* expressing ALFA tagged RpoC or MmpL3 with a TurboID-NBALFA fusion.

(A) Immunoblots of lysates from WT *M. smegmatis*, MGM7085 (no ALFA), MGM7105 (encoding RpoC-ALFA), MGM7081 (encoding MmpL3-ALFA), all with a tet inducible TurboID-NBALFA. Lanes 2-4 are uninduced and lanes 5-7 were induced with ATc-50ng/ml for 3 hours. The blot was probed with anti-BirA then anti-rabbit Ig-HRP.

(B) Streptavidin-HRP probed blot to detect biotinylated proteins in WT, no ALFA, RpoC-ALFA and MmpL3-ALFA, all expressing TurboID-NBALFA after biotin labeling. Black arrowheads indicate biotinylated proteins at the predicted size of RpoC-ALFA (lane 3) or MmpL3-ALFA (lane 4)

(C) Volcano plot of RpoC-ALFA compared to No ALFA proximity labeling. Blue points indicate Log2FC>1 and Adjusted P-value <0.05. Significant blue points labeled with protein names, including RpoC bait protein.

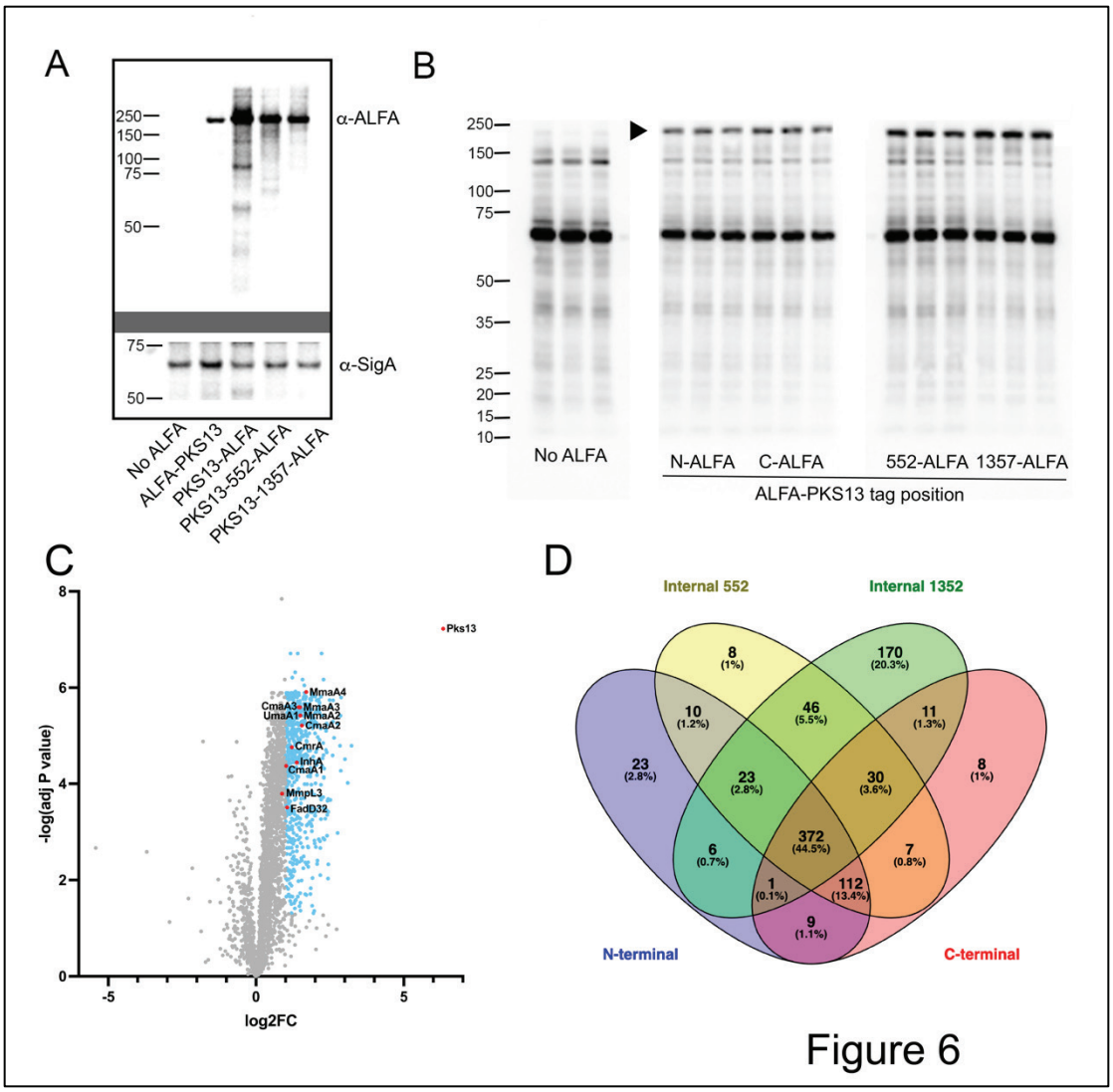

Figure 6. Proximity labeling of *M. tuberculosis* PKS13

(A) Immunoblots of strains expressing ALFA tagged PKS13 proteins: no ALFA tag, N-terminal ALFA tagged PKS13, C-terminal ALFA tagged PKS13, internal ALFA tag (552AA) PKS13, and Internal ALFA tag (1357AA) PKS13. Top probed using NBALFA then anti-VHH-HRP. Bottom blot reprobed with anti-SigA then anti-rabbit Ig-HRP.

(B) Streptavidin-HRP detection of biotinylated proteins in triplicate proximity labeling experiments in *M. tuberculosis* no ALFA control, N-terminal ALFA tagged PKS13, C-terminal ALFA tagged PKS13, internal ALFA tag (552AA) PKS13, and internal ALFA tag (1357AA) PKS13. Arrowhead indicates a biotinylated protein of approximate bait (PKS13) size.

528 **(C)** Volcano plots of proximity labeling samples N-terminal ALFA-PKS13 compared to No ALFA.
529 Blue points indicate Log2FC>1 and Adjusted P-value <0.05. with red points highlighting proteins
530 with known functions in mycolic acid biosynthesis.
531
532 **(D)** Venn diagram depicting position specific proximity interactome (Log2FC > 1 and Adjusted P-
533 value < 0.001) of PKS13 (also see Table S5 for specific protein lists).
534

535 **Bibliography**
536

537 1. WHO. 2024. Global Tuberculosis Report 2024.
538 2. van Kessel JC, Hatfull GF. 2008. Efficient point mutagenesis in mycobacteria using
539 single-stranded DNA recombineering: characterization of antimycobacterial drug targets.
540 Mol Microbiol 67:1094-107.
541 3. van Kessel JC, Hatfull GF. 2007. Recombineering in Mycobacterium tuberculosis. Nat
542 Methods 4:147-52.
543 4. Stover CK, de la Cruz VF, Fuerst TR, Burlein JE, Benson LA, Bennett LT, Bansal GP,
544 Young JF, Lee MH, Hatfull GF, et al. 1991. New use of BCG for recombinant vaccines.
545 Nature 351:456-60.
546 5. Bosch B, DeJesus MA, Poulton NC, Zhang W, Engelhart CA, Zaveri A, Lavalette S,
547 Ruecker N, Trujillo C, Wallach JB, Li S, Ehrt S, Chait BT, Schnappinger D, Rock JM.
548 2021. Genome-wide gene expression tuning reveals diverse vulnerabilities of M.
549 tuberculosis. Cell 184:4579-4592 e24.
550 6. Rock JM, Hopkins FF, Chavez A, Diallo M, Chase MR, Gerrick ER, Pritchard JR, Church
551 GM, Rubin EJ, Sassetti CM, Schnappinger D, Fortune SM. 2017. Programmable
552 transcriptional repression in mycobacteria using an orthogonal CRISPR interference
553 platform. Nat Microbiol 2:16274.
554 7. Yan MY, Li SS, Ding XY, Guo XP, Jin Q, Sun YC. 2020. A CRISPR-Assisted
555 Nonhomologous End-Joining Strategy for Efficient Genome Editing in Mycobacterium
556 tuberculosis. mBio 11.
557 8. Lazar N, Fay A, Nandakumar M, Boyle KE, Xavier J, Rhee K, Glickman MS. 2017.
558 Control of biotin biosynthesis in mycobacteria by a pyruvate carboxylase dependent
559 metabolic signal. Mol Microbiol 106:1018-1031.
560 9. Murphy KC, Nelson SJ, Nambi S, Papavinasasundaram K, Baer CE, Sassetti CM. 2018.
561 ORBIT: a New Paradigm for Genetic Engineering of Mycobacterial Chromosomes. mBio
562 9.
563 10. Kang CM, Nyayapathy S, Lee JY, Suh JW, Husson RN. 2008. Wag31, a homologue of
564 the cell division protein DivIVA, regulates growth, morphology and polar cell wall
565 synthesis in mycobacteria. Microbiology (Reading) 154:725-735.
566 11. Fay A, Glickman MS. 2014. An essential nonredundant role for mycobacterial DnaK in
567 native protein folding. PLoS Genet 10:e1004516.
568 12. Sukumar N, Tan S, Aldridge BB, Russell DG. 2014. Exploitation of Mycobacterium
569 tuberculosis reporter strains to probe the impact of vaccination at sites of infection. PLoS
570 Pathog 10:e1004394.
571 13. Holowka J, Trojanowski D, Ginda K, Wojtas B, Gielniewski B, Jakimowicz D,
572 Zakrzewska-Czerwinska J. 2017. HupB Is a Bacterial Nucleoid-Associated Protein with
573 an Indispensable Eukaryotic-Like Tail. mBio 8.
574 14. Judd JA, Canestrari J, Clark R, Joseph A, Lapierre P, Lasek-Nesselquist E, Mir M,
575 Palumbo M, Smith C, Stone M, Upadhyay A, Wirth SE, Dedrick RM, Meier CG, Russell
576 DA, Dills A, Dove E, Kester J, Wolf ID, Zhu J, Rubin ER, Fortune S, Hatfull GF, Gray TA,
577 Wade JT, Derbyshire KM. 2021. A Mycobacterial Systems Resource for the Research
578 Community. mBio 12.
579 15. Zhu J, Wolf ID, Dulberger CL, Won HI, Kester JC, Judd JA, Wirth SE, Clark RR, Li Y,
580 Luo Y, Gray TA, Wade JT, Derbyshire KM, Fortune SM, Rubin EJ. 2021. Spatiotemporal
581 localization of proteins in mycobacteria. Cell Rep 37:110154.
582 16. Hink MA, Griep RA, Borst JW, van Hoek A, Eppink MH, Schots A, Visser AJ. 2000.
583 Structural dynamics of green fluorescent protein alone and fused with a single chain Fv
584 protein. J Biol Chem 275:17556-60.

585 17. Pedelacq JD, Cabantous S, Tran T, Terwilliger TC, Waldo GS. 2006. Engineering and
586 characterization of a superfolder green fluorescent protein. Nat Biotechnol 24:79-88.
587 18. Niinae T, Ishihama Y, Imami K. 2021. Biotinylation-based proximity labelling proteomics:
588 basics, applications and technical considerations. J Biochem 170:569-576.
589 19. Lam SS, Martell JD, Kamer KJ, Deerinck TJ, Ellisman MH, Mootha VK, Ting AY. 2015.
590 Directed evolution of APEX2 for electron microscopy and proximity labeling. Nat
591 Methods 12:51-4.
592 20. Martell JD, Deerinck TJ, Sancak Y, Poulos TL, Mootha VK, Sosinsky GE, Ellisman MH,
593 Ting AY. 2012. Engineered ascorbate peroxidase as a genetically encoded reporter for
594 electron microscopy. Nat Biotechnol 30:1143-8.
595 21. Branon TC, Bosch JA, Sanchez AD, Udeshi ND, Svinkina T, Carr SA, Feldman JL,
596 Perrimon N, Ting AY. 2018. Efficient proximity labeling in living cells and organisms with
597 TurboID. Nat Biotechnol 36:880-887.
598 22. Roux KJ, Kim DI, Raida M, Burke B. 2012. A promiscuous biotin ligase fusion protein
599 identifies proximal and interacting proteins in mammalian cells. J Cell Biol 196:801-10.
600 23. Ganapathy US, Bai L, Wei L, Eckartt KA, Lett CM, Previti ML, Carrico IS, Seeliger JC.
601 2018. Compartment-Specific Labeling of Bacterial Periplasmic Proteins by Peroxidase-
602 Mediated Biotinylation. ACS Infect Dis 4:918-925.
603 24. Jaisinghani N, Previti ML, Andrade J, Askenazi M, Ueberheide B, Seeliger JC. 2024.
604 Proteomics from compartment-specific APEX2 labeling in Mycobacterium tuberculosis
605 reveals Type VII secretion substrates in the cell wall. Cell Chem Biol 31:523-533 e4.
606 25. Veyron-Churlet R, Saliou JM, Locht C. 2021. Interconnection of the mycobacterial
607 heparin-binding hemagglutinin with cholesterol degradation and heme/iron pathways
608 identified by proximity-dependent biotin identification in Mycobacterium smegmatis.
609 Environ Microbiol 23:3212-3224.
610 26. Gotzke H, Kilisch M, Martinez-Carranza M, Sograte-Idrissi S, Rajavel A, Schlichthaerle
611 T, Engels N, Jungmann R, Stenmark P, Opazo F, Frey S. 2019. The ALFA-tag is a highly
612 versatile tool for nanobody-based bioscience applications. Nat Commun 10:4403.
613 27. Arbabi-Ghahroudi M, Tanha J, MacKenzie R. 2005. Prokaryotic expression of antibodies.
614 Cancer Metastasis Rev 24:501-19.
615 28. Harris KK, Fay A, Yan HG, Kunwar P, Socci ND, Pottabathini N, Juventhala RR,
616 Djaballah H, Glickman MS. 2014. Novel imidazoline antimicrobial scaffold that inhibits
617 DNA replication with activity against mycobacteria and drug resistant Gram-positive
618 cocci. ACS Chem Biol 9:2572-83.
619 29. Fay A, Czudnochowski N, Rock JM, Johnson JR, Krogan NJ, Rosenberg O, Glickman
620 MS. 2019. Two Accessory Proteins Govern MmpL3 Mycolic Acid Transport in
621 Mycobacteria. mBio 10.
622 30. Carel C, Nukdee K, Cantaloube S, Bonne M, Diagne CT, Laval F, Daffe M, Zerbib D.
623 2014. Mycobacterium tuberculosis proteins involved in mycolic acid synthesis and
624 transport localize dynamically to the old growing pole and septum. PLoS One 9:e97148.
625 31. Wu W, Xing L, Zhou B, Lin Z. 2011. Active protein aggregates induced by terminally
626 attached self-assembling peptide ELK16 in Escherichia coli. Microb Cell Fact 10:9.
627 32. Dey S, Lane JM, Lee RE, Rubin EJ, Sacchettini JC. 2010. Structural characterization of
628 the Mycobacterium tuberculosis biotin biosynthesis enzymes 7,8-diaminopelargonic acid
629 synthase and dethiobiotin synthetase. Biochemistry 49:6746-60.
630 33. Salaemae W, Azhar A, Booker GW, Polyak SW. 2011. Biotin biosynthesis in
631 Mycobacterium tuberculosis: physiology, biochemistry and molecular intervention.
632 Protein Cell 2:691-5.
633 34. Oh TJ, Daniel J, Kim HJ, Sirakova TD, Kolattukudy PE. 2006. Identification and
634 characterization of Rv3281 as a novel subunit of a biotin-dependent acyl-CoA
635 Carboxylase in Mycobacterium tuberculosis H37Rv. J Biol Chem 281:3899-908.

636 35. Daniel J, Oh TJ, Lee CM, Kolattukudy PE. 2007. AccD6, a member of the Fas II locus, is
637 a functional carboxyltransferase subunit of the acyl-coenzyme A carboxylase in
638 Mycobacterium tuberculosis. J Bacteriol 189:911-7.
639 36. Rhee KY, Erdjument-Bromage H, Tempst P, Nathan CF. 2005. S-nitroso proteome of
640 Mycobacterium tuberculosis: Enzymes of intermediary metabolism and antioxidant
641 defense. Proc Natl Acad Sci U S A 102:467-72.
642 37. Portevin D, De Sousa-D'Auria C, Houssin C, Grimaldi C, Chami M, Daffe M, Guilhot C.
643 2004. A polyketide synthase catalyzes the last condensation step of mycolic acid
644 biosynthesis in mycobacteria and related organisms. Proc Natl Acad Sci U S A 101:314-
645 9.
646 38. Bon C, Cabantous S, Julien S, Guillet V, Chalut C, Rima J, Brison Y, Malaga W,
647 Sanchez-Dafun A, Gavalda S, Quemard A, Marcoux J, Waldo GS, Guilhot C, Mourey L.
648 2022. Solution structure of the type I polyketide synthase Pks13 from Mycobacterium
649 tuberculosis. BMC Biol 20:147.
650 39. Kim SK, Dickinson MS, Finer-Moore J, Guan Z, Kaake RM, Echeverria I, Chen J, Pulido
651 EH, Sali A, Krogan NJ, Rosenberg OS, Stroud RM. 2023. Structure and dynamics of the
652 essential endogenous mycobacterial polyketide synthase Pks13. Nat Struct Mol Biol
653 30:296-308.
654 40. Tudo G, Laing K, Mitchison DA, Butcher PD, Waddell SJ. 2010. Examining the basis of
655 isoniazid tolerance in nonreplicating Mycobacterium tuberculosis using transcriptional
656 profiling. Future Med Chem 2:1371-83.
657 41. Wilson M, DeRisi J, Kristensen HH, Imboden P, Rane S, Brown PO, Schoolnik GK.
658 1999. Exploring drug-induced alterations in gene expression in Mycobacterium
659 tuberculosis by microarray hybridization. Proc Natl Acad Sci U S A 96:12833-8.
660 42. Cabruja M, Mondino S, Tsai YT, Lara J, Gramajo H, Gago G. 2017. A conditional mutant
661 of the fatty acid synthase unveils unexpected cross talks in mycobacterial lipid
662 metabolism. Open Biol 7.
663 43. Ahamed M, Jaisinghani N, Li M, Winkeler I, Silva S, Previti ML, Seeliger JC. 2022.
664 Optimized APEX2 peroxidase-mediated proximity labeling in fast- and slow-growing
665 mycobacteria. Methods Enzymol 664:267-289.
666 44. Snapper SB, Melton RE, Mustafa S, Kieser T, Jacobs WR, Jr. 1990. Isolation and
667 characterization of efficient plasmid transformation mutants of Mycobacterium
668 smegmatis. Mol Microbiol 4:1911-9.
669 45. Yin Y, Feng X, Yu H, Fay A, Kovach A, Glickman MS, Li H. 2021. Structural basis for
670 aggregate dissolution and refolding by the Mycobacterium tuberculosis ClpB-DnaK bi-
671 chaperone system. Cell Rep 35:109166.
672

673

SI Figures

Figures S1-S3

Supplementary Tables

Table S1: Strains, plasmids, oligos, and DNA sequences used in this study.

Table S2: RpoC-ALFA vs no ALFA control proximity data. Analysis of biotinylated peptides from proximity labeled lysates made from *M. smegmatis* strains MGM7106 and MGM7085.

Table S3: PKS13-ALFA (4 tag positions) vs no ALFA control proximity data. Analysis of biotinylated peptides from proximity labeled lysates made from *M. tuberculosis* strains MGM7416, MGM7418, MGM7419, MGM7420, and MGM7421.

Table S4: 15 sample proteins involved with mycolic acid synthesis and transport. Log2FC and Adjusted P-values for all 4 ALFA tag positions shown. Highlighted in green are Log2FC>1.

Table S5: List of PKS13-ALFA proximity hits with Log2FC>1 and adjusted P-value<0.0001 used for generating Venn diagram (Figure 6D).

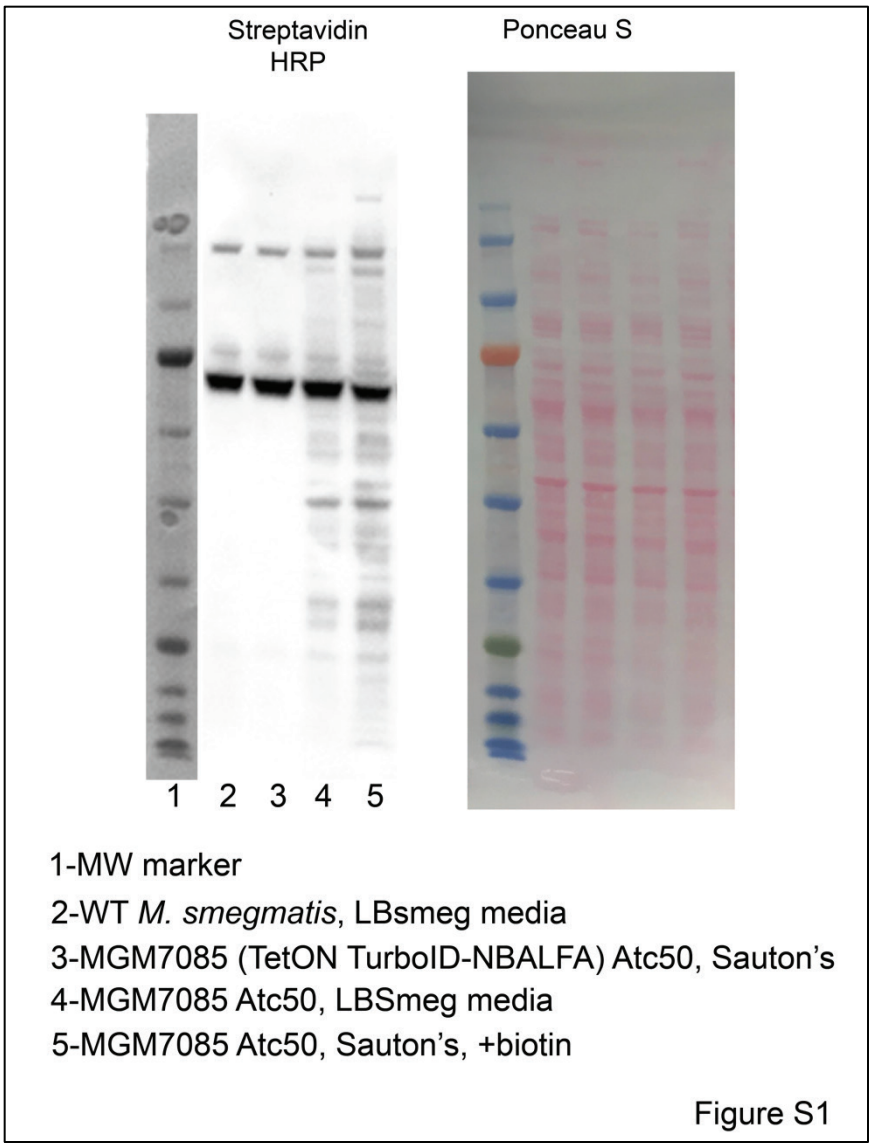

Figure S1

Streptavidin HRP blot (left) and ponceau S staining (right) of the indicated strains and growth conditions showing levels of endogenous biotinylated proteins in *M. smegmatis*.

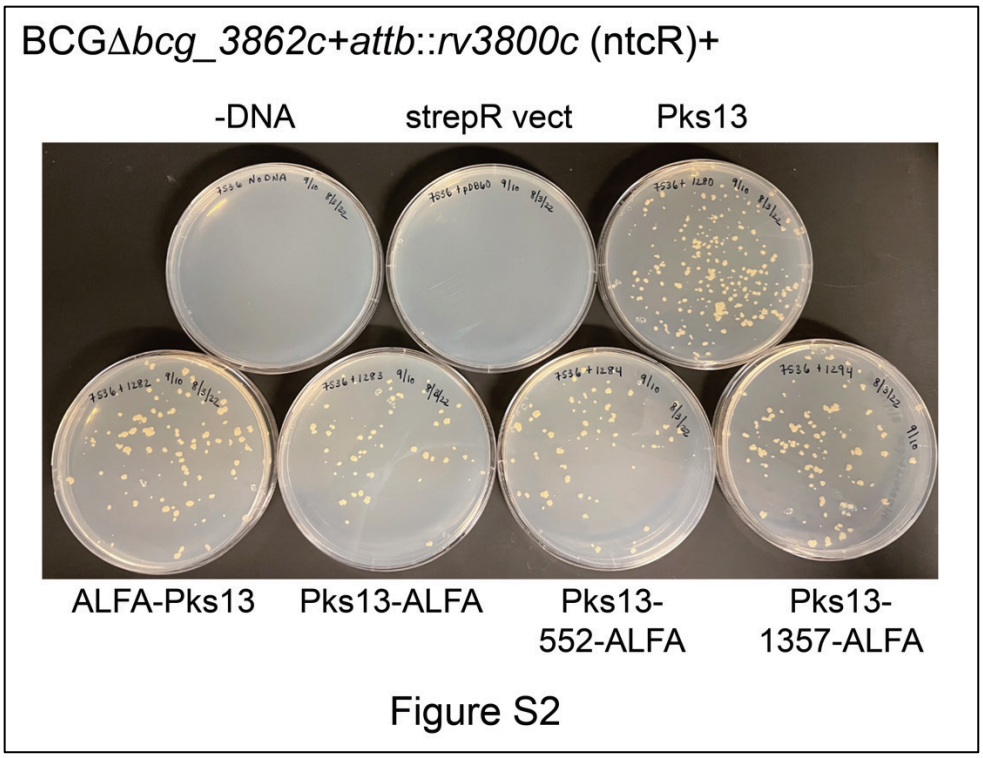

Figure S2

Functionality testing of PKS13-ALFA alleles via *attB* allelic exchange.

Shown are streptomycin agar media with transformation of a merodiploid BCG strain with a chromosomal deletion of *pks13* (*BCG_3862c*) and a second copy of M. tuberculosis *rv3800c* at the *attB* site conferring nourseothricin-resistance. Transformation of this strain with an *attB* integrating vector conferring streptomycin-resistance encoding nothing (strepR vect) or alleles of *pks13* with no ALFA tag, or four different ALFA tag position in the PKS13 protein.

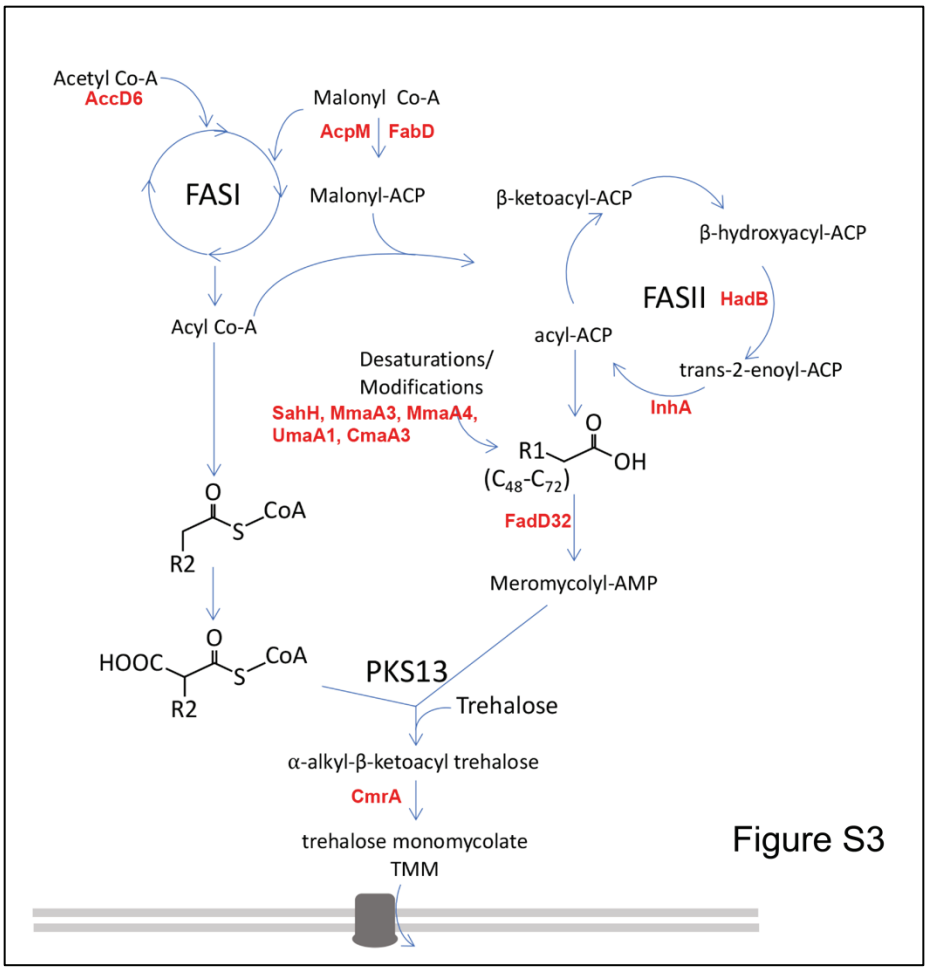

Figure S3. PKS13-ALFA proximity labeled hits within the mycolic acid biosynthesis pathway. Proteins found in all four ALFA tagged labeling conditions with a Log2FC >1.3 and adjusted P-value < 0.05 in bold, red font.